Bioactive Materials 30 (2023) 169–183

Contents lists available at ScienceDirect

Bioactive Materials

journal homepage: www.keaipublishing.com/en/journals/bioactive-materials

Dual-engineered cartilage-targeting extracellular vesicles derived from mesenchymal stem cells enhance osteoarthritis treatment via miR-223/NLRP3/pyroptosis axis: Toward a precision therapy

Weixuan Liu [a,b,1], Anqi Liu [d,e,1], Xujun Li [f,1], Ziyang Sun [b,c], Zhenghua Sun [b], Yaru Liu [b], Gang Wang [b], Dan Huang [b], Hao Xiong [b,c,****], Shiyang Yu [b,c,***], Xintao Zhang [a,**], Cunyi Fan [b,c,*]

[a] Department of Sports Medicine, Peking University Shenzhen Hospital, Shenzhen Peking University-The Hong Kong University of Science and Technology Medical Center, Shenzhen, 518036, China
[b] Shanghai Engineering Research Center for Orthopedic Material Innovation and Tissue Regeneration, Shanghai, 201306, China
[c] Department of Orthopedics, Shanghai Sixth People's Hospital Affiliated to Shanghai Jiao Tong University School of Medicine, Shanghai, 200233, China
[d] Department of Orthodontics, Shanghai Stomatological Hospital & School of Stomatology, Fudan University, Shanghai, 200001, China
[e] Shanghai Key Laboratory of Craniomaxillofacial Development and Diseases, Fudan University, Shanghai, 200001, China
[f] Minhang Hospital, Fudan University, Shanghai, 201199, China

ARTICLE INFO

Keywords:
Osteoarthritis
Extracellular vesicles
NLRP3 inflammasome
Pyroptosis
Cartilage-targeting

ABSTRACT

Osteoarthritis (OA) is the most common disabling joint disease with no effective disease modifying drugs. Extracellular vesicles released by several types of mesenchymal stem cells could promote cartilage repair and ameliorate OA pathology in animal models, representing a novel therapeutic strategy. In this study, we demonstrated that extracellular vesicles derived from human umbilical cord mesenchymal stem cells (hUC-EVs) could maintain chondrocyte homeostasis and alleviate OA, and further revealed a novel molecular mechanism of this therapeutic effect. miR-223, which could directly bind with the 3′UTR of NLRP3 mRNA, was found to be a key miRNA for hUC-EVs to exert beneficial effects on inflammation inhibiting and cartilage protecting. For enhancing the effect on mitigating osteoarthritis, exogenous miR-223 was loaded into hUC-EVs by electroporation, and a collagen II-targeting peptide (WYRGRL) was modified onto the surface of hUC-EVs by genetic engineering to achieve a more targeted and efficient RNA delivery to the cartilage. The dual-engineered EVs showed a maximal effect on inhibiting the NLRP3 inflammasome activation and chondrocyte pyroptosis, and offered excellent results for the treatment of OA. This study provides a novel theoretical basis and a promising therapeutic strategy for the application of engineered extracellular vesicles in OA treatment.

1. Introduction

Osteoarthritis (OA) is the most common type of degenerative joint disease, with 250 million people currently suffered [1,2]. The major pathogenesis of OA is progressive cartilage degradation, synovial inflammation and abnormal subchondral bone remodeling [3,4], in

Peer review under responsibility of KeAi Communications Co., Ltd.
* Corresponding author. Department of Orthopedics, Shanghai Sixth People's Hospital Affiliated to Shanghai Jiao Tong University School of Medicine, Shanghai, 200233, China.
** Corresponding author. Department of Sports Medicine, Peking University Shenzhen Hospital, Shenzhen Peking University-The Hong Kong University of Science and Technology Medical Center, Shenzhen, 518036, China.
*** Corresponding author. Department of Orthopedics, Shanghai Sixth People's Hospital Affiliated to Shanghai Jiao Tong University School of Medicine, Shanghai, 200233, China.
**** Corresponding author. Department of Orthopedics, Shanghai Sixth People's Hospital Affiliated to Shanghai Jiao Tong University School of Medicine, Shanghai, 200233, China.
E-mail addresses: 15870679103@163.com (H. Xiong), yushiyangysy@126.com (S. Yu), zhangxintao@sina.com (X. Zhang), cyfan@sjtu.edu.cn (C. Fan).
[1] These authors contributed equally to this work.

https://doi.org/10.1016/j.bioactmat.2023.06.012
Received 22 November 2022; Received in revised form 24 May 2023; Accepted 19 June 2023

which the impaired homeostasis of chondrocytes plays a key role. OA leads to persistent pain, joint stiffness, and physical disability, imposing a tremendous burden on health care systems. Current OA treatments are limited and insufficient to prevent its onset and progression, making the development of new therapeutic strategies all the more important and urgent [5]. Therapies based on mesenchymal stem cells (MSCs) represent a new generation of cartilage regeneration and OA treatment [6,7]. In recent years, accumulating evidence suggests that MSC-derived extracellular vesicles (MSC-EVs) are the key biological mediators through which MSCs exert their functions in immunomodulation and tissue regeneration [8], and significant previous studies have demonstrated the therapeutic effects of MSC-EVs in animal models of OA [9,10].

Umbilical cords are an excellent source of MSCs for the cost-effectiveness, acceptability, and universality [11,12]. Compared to other MSCs, human umbilical cord mesenchymal stem cells (hUCMSCs) have biological advantages for being more primitive, proliferative, and immunosuppressive [13,14], and are considered to have broad application prospects [15,16]. hUCMSC-derived extracellular vesicles (hUC-EVs) have emerged as a promising treatment for various degenerative and inflammatory diseases due to its unique advantages. Previous studies showed that hUC-EVs could be used to treat a variety of illnesses, such as inflammatory bowel disease [17], type-2 diabetes [18], heart failure [19], and wound inflammation [20]. While hUC-EVs represent a potential strategy for promoting tissue repair and inhibiting inflammation, to date, they have been rarely studied and applied in OA therapy. Hence, the first objective of this study was to determine the therapeutic potential of hUC-EVs in the treatment of OA.

As natural EVs may not be able to provide sufficient and optimal curative effects in various disease conditions, bioengineered EVs have been increasingly explored [21,22]. EVs can be loaded with therapeutic cargos by both the exogenous methods, such as co-incubation and electroporation, and the endogenous methods, like genetically modifying the parental cell to regulate the specific RNA or protein [23]. A variety of EVs, specifically loaded with therapeutic RNA molecules [24], proteins [25] and small molecule drugs [26] have been developed. Also, the surface property of EVs could be engineered to enable specific targeting or mediate a certain biological function. For instance, the engineered EVs achieved by fusing brain-targeting peptide to the extra-exosomal N terminus of Lamp2b, a protein on exosomal membranes, showed a promising targeting capability and therapeutic effect for Alzheimer's disease [27]. As precision medicine develops, in order to maximize therapeutic effects, both targeting abilities toward pathological tissues as well as freely assembled agents based on disease-specific mechanisms are continually being demanded. Therefore, the second aim of this study was to reveal an underlying mechanism of the treatment effect of hUC-EVs on OA, and develop dual-engineered EVs (both the content and surface) accordingly to achieve a better and more precise treatment.

Inflammasomes are associated with inflammation-related disorders in many systems [28], including inflammatory bowel disease [29], Parkinson's disease [30], myocardial infarction [31], etc. The best characterized is the NLRP3 inflammasome [32], a cytosolic protein complex. Under stimulation, the NLRP3 inflammasomes are assembled and activated, cleaving pro-caspase-1 into caspase-1, which then activates inflammatory cytokines pro-IL-1β into IL-1β, pro-IL-18 into IL-18, the secreted form [33]. Meanwhile, the NLRP3 inflammasomes trigger cell pyroptosis by initiating the cleavage of gasdermin D (GSDMD), which forms pores on the cell membrane [34]. The overactivation of NLRP3 inflammasomes promotes the development and progression of inflammatory diseases [35], and has recently been proposed to be a key event in the pathogenesis of OA [36–39], thus its inhibition may serve as a therapeutic target. Yet, studies specifically investigating the therapeutic effect of NLRP3 inflammasome inhibition in OA are very scarce.

In this study, we first demonstrated that hUC-EVs promoted cartilage homeostasis and alleviate OA in vivo *and* in vitro. MiRNAs are one of the most important contents of EVs, which regulate gene expression post-transcriptionally [40]. We carried out deep miRNA sequencing analysis between OA cartilage tissues treated with hUC-EVs and negative control (PBS) to reveal the possible molecular mechanisms of the therapeutic effect of hUC-EVs on OA. We found that hUC-EVs led to higher expressions of miR-223 in rat cartilage, which could directly bind with the 3′ untranslated region (3′UTR) of NLRP3 mRNA and inhibit the activation of NLRP3 inflammasome. Thus, for enhancing the effect of hUC-EVs on mitigating osteoarthritis, exogenous miR-223 was loaded into hUC-EVs by electroporation to increase its content. Recently, several studies demonstrated that targeting delivery of agents to cartilage might be effective for OA therapy, and various peptides with specific affinity to cartilage received increasing attention [41,42]. WYRGRL, one of the collagen II-targeting peptides (CTP), was reported to increase the cartilage-targeting efficiency of nanoparticles by about 72-fold in vivo [43]. Based on this, WYRGRL expressed with Lamp2b protein was modified onto the surface of hUC-EVs to achieve a more targeted and efficient delivery to the cartilage in this study. Using the two engineering methods mentioned above, we harvested three kinds of engineered hUC-EVs, CTP-EVs with cartilage-targeting peptide expressed on the external surface, Mir-EVs that loaded with miR-223, and CTP/Mir-EVs which possess both characters. Last, we verified that the dual-engineered CTP/Mir-EVs maximized the effect of cartilage repairing by targeted RNA delivery to cartilage, inhibiting the NLRP3 inflammasome activation and chondrocyte pyroptosis. Our findings unravel an underlying signal pathway of OA progression, offering therapeutic targets and a promising direction for the translational application in clinical practice (Scheme 1).

2. Results and discussion

2.1. Identification and characterization of hUCMSCs and hUC-EVs

hUCMSCs displayed good proliferation capability and typical spindle-like morphology (Fig. 1A). For the tri-lineage differentiation potential, hUCMSCs were able to successfully differentiate into the osteogenic (Fig. 1B, left panel, Alizarin Red staining), adipogenic (Fig. 1B, middle panel, Oil Red O staining), and chondrogenic lineages in respective medium (Fig. 1B, right panel, Alcian Blue staining). Expressions of the MSC surface markers were analyzed using flow cytometry, showing that hUCMSCs were positive for CD73 and CD90, and negative for CD34 and CD45 (Fig. 1C).

Transmission electron microscopy (TEM) revealed that hUC-EVs exhibited a typical spherical bilayer membrane structure (Fig. 1D). Nanoparticle Tracking Analysis (NTA) of these vesicles indicated an average diameter of 142.9 nm, and the main peak of particle size was 131.3 nm (Fig. 1E). In addition, the concentration was about 2.2×10^{10} particles/ml. Further, western blotting revealed that exosomal specific markers (CD81, Tsg101, Alix) were positive, while Calnexin was negative (Fig. 1F). The above results indicated that EVs were successfully isolated from hUCMSCs.

2.2. hUC-EVs promote cell survival and anabolism of IL-1β-induced chondrocytes

We then investigated the effect of hUC-EVs on chondrocytes in vitro, and the experimental schematic is shown in Fig. 2A. The cellular uptake of DiO-stained hUC-EVs was observed under confocal fluorescence microscope after co-incubation for 12 h with chondrocytes (Fig. 2B, negative control in Fig. S1), which showed the DiO-stained hUC-EVs entered chondrocytes successfully. IL-1β (10 ng/mL, all the same below) was used to imitate the inflammatory microenvironment of OA [44]. IL-1β-induced chondrocytes were treated with hUC-EVs (5×10^8 particles/ml, *hUC-EVs group*) or normal medium (*IL-1β group*) for 24 h. The results of cell counting kit-8 (CCK-8) assay showed that hUC-EVs could partially reverse IL-1β-decreased chondrocytes viability (Fig. 2C).

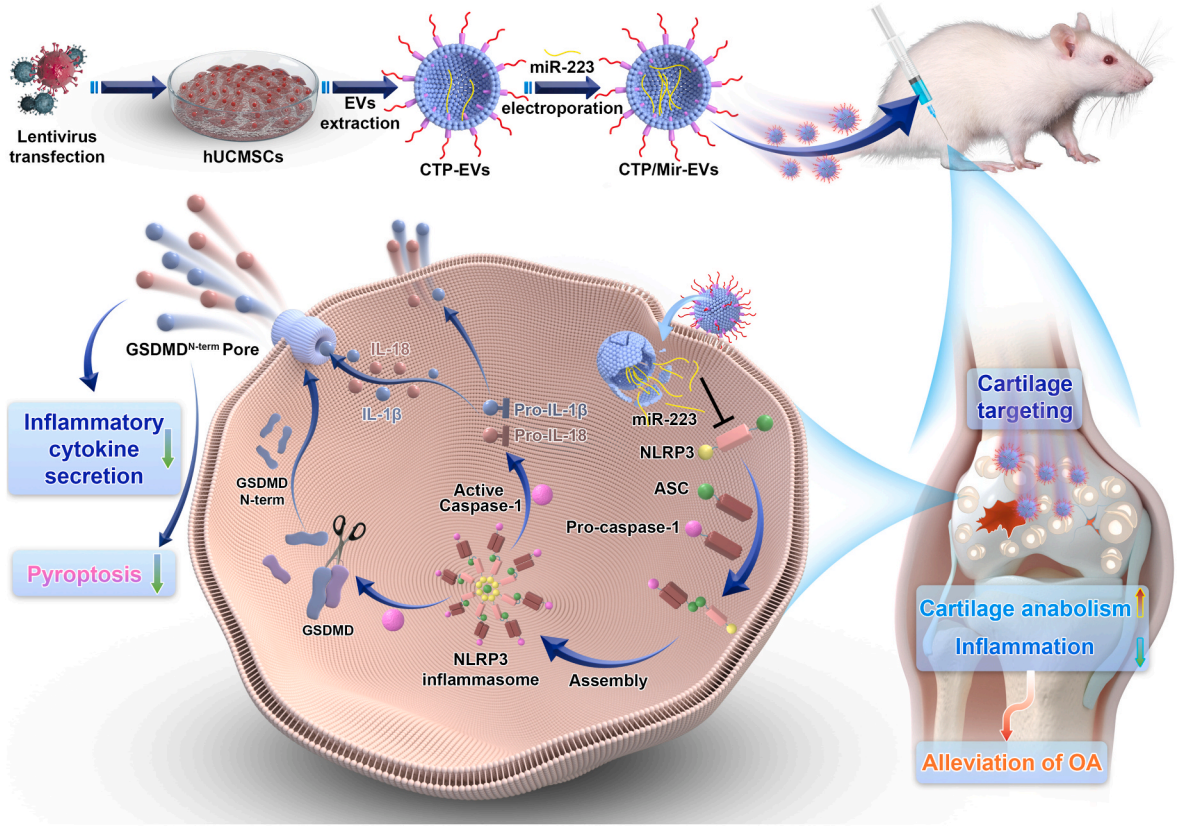

Scheme 1. A schematic overview of the study.

Meanwhile, the protein levels of cartilage anabolic factors (Collagen II and SOX9) and catabolic factor (matrix metalloproteinase 13, MMP13), which were highly related to the pathology of OA [45,46], were measured by western blotting. Consistent with former studies [47,48], IL-1β treatment significantly reduced Collagen II and SOX9 expression, while upregulated the level of MMP13. The supplement of hUC-EVs reversed the effect of IL-1β on chondrocytes (Fig. 2D and E). The results of immunofluorescence staining (Collagen II and Aggrecan) also supported the findings (Fig. 2F–H). In summary, hUC-EVs could promote cell survival and anabolism of IL-1β-treated chondrocytes.

2.3. *hUC-EVs alleviate the inflammation and cartilage degeneration in OA rat model*

To evaluate the role of hUC-EVs on articular cartilage protection, the monosodium iodoacetate (MIA)-induced OA model of rat was carried out. The schematic diagram of animal experiments is shown in Fig. 3A. The OA rat knees were treated with 10 μL negative control (*PBS group*) or 10 μL hUC-EVs (10^{10} particles/ml, diluted in PBS) (*hUC-EVs group*) once a week for 4 times 1 week after the MIA injection. The knee joints were harvested and examined at 5 weeks. Pro-inflammatory factors in the cartilage, which play key roles in OA progression, were measured by ELISA, including IL-1β, MMP2, tumor necrosis factor α (TNF-α), prostaglandins E2 (PGE2), etc [49]. The results suggested that hUC-EVs markedly inhibited the generation of IL-1β, MMP2, TNF-α, and PGE2 compared to the PBS group (Fig. 3B).

The cartilage degradation, characterized by gradual loss of collagen II, aggrecan, and proteoglycan in extracellular matrix (ECM), is a typical pathological manifestation of OA [50]. The mRNA levels of anabolic factors (Collagen II, SOX9), and catabolic factor (MMP13) were measured using qRT-PCR, which showed that hUC-EVs could reverse the inhibition of cartilage anabolism induced by MIA (Fig. 3C). Histological analyses, including Hematoxylin-eosin (H&E) staining, Safranin O/Fast Green staining (aggrecan and proteoglycan), and immunohistochemical staining (collagen II) of knee joint sections were performed. As the representative images shown in Fig. 3D, the control group showed normal structures of the articular cartilage, with smooth surfaces, and aggrecan, proteoglycan, and collagen II were uniformly distributed. In the PBS group, articular cartilage was obviously degenerated after MIA injection, with ECM loss, representing the progression of OA. The changes were partly rescued in the EVs-treated group, in which the aggrecan, proteoglycan, and collagen II were obviously upregulated compared to the PBS group. The maximal and summed scores of the Osteoarthritis Research Society International (OARSI) scoring system (Fig. 3E), as well the Mankin's score (Fig. 3F), were evaluated to quantify the severity of cartilage degeneration. Moreover, Collagen II protein levels in articular cartilage were assessed using the immunohistochemical staining results (Fig. 3G). Collectively, these results revealed that hUC-EVs injection could significantly inhibit inflammation, and alleviate the cartilage degradation in MIA-induced OA models.

2.4. *miR-223 mediates the inhibitory effect of hUC-EVs on NLRP3 inflammasome*

To further investigate the underlying mechanism of hUC-EVs promoting chondrocyte survival and cartilage repair, we performed high-throughput miRNA sequencing (service provided by BGI, Shenzhen) of cartilage tissues in the PBS group and hUC-EVs group. As the volcano map demonstrates, 12 miRNAs were upregulated and 30 downregulated in the hUC-EVs group (Fig. 4A), and the details of the miRNA differential expression are presented in the heat map (Fig. 4B). In recent years, cell pyroptosis and NLRP3 inflammasome has attracted increasing attention for their roles in promoting OA progression and cartilage degeneration [36,37,51]. The assembling of NLRP3 inflammasome activates Caspase-1, which then leads to the release of pro-inflammatory cytokines IL-18 and IL-1β, as well as gasdermin D (GSDMD)-triggered cell

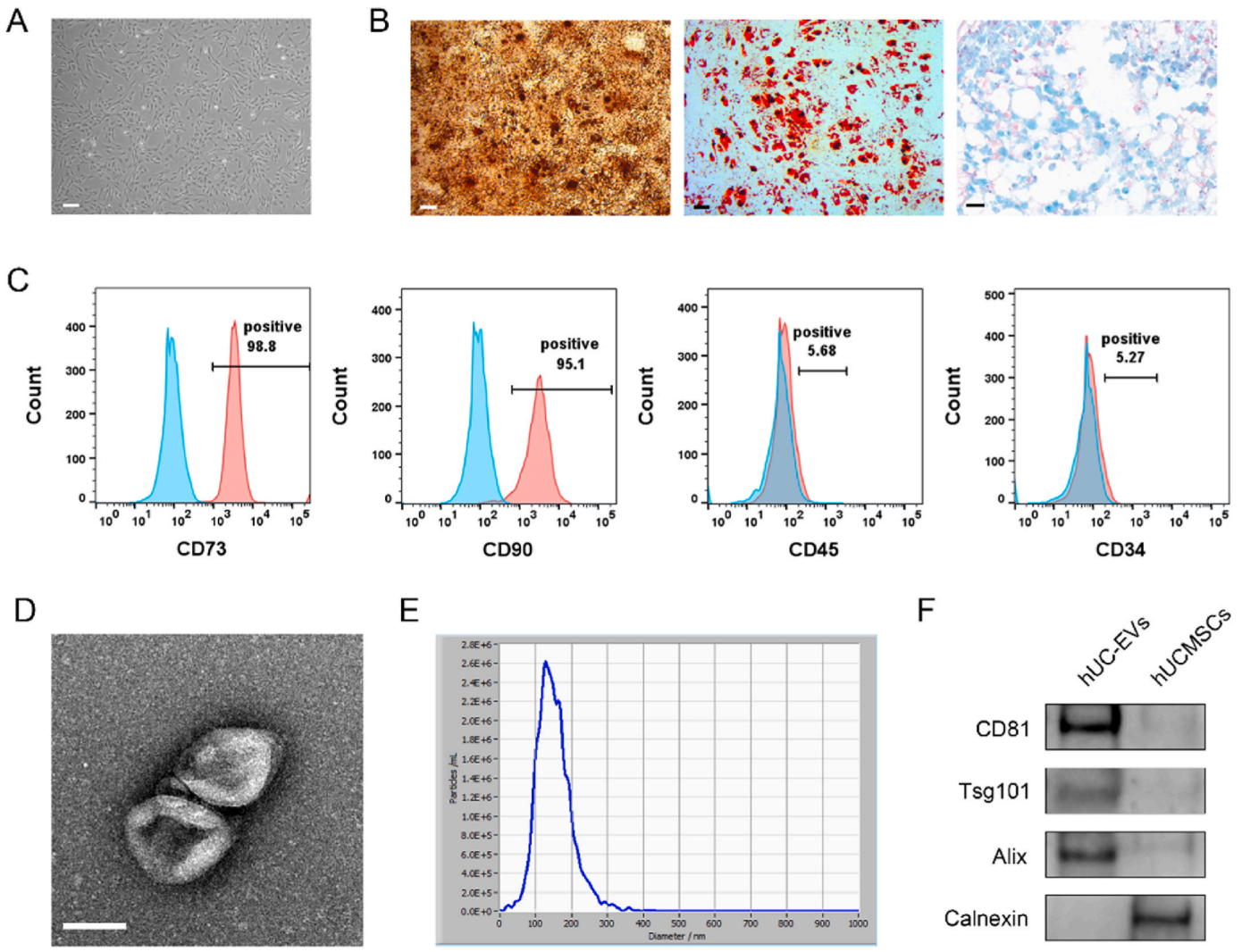

Fig. 1. Identification and characterization of hUCMSCs and hUC-EVs
(A) hUCMSCs displayed a representative spindle-like morphology. Scale bar: 100 μm. (B) Osteogenesis, adipogenesis, and chondrogenesis were all capable of being induced in hUCMSCs. Alizarin Red S staining, scale bar: 100 μm. Oil Red O staining, scale bar: 100 μm. Alcian Blue staining, scale bar: 25 μm. (C) Flow cytometric analysis of mesenchymal positive markers (CD73, CD90) and negative markers (CD34, CD45). Isotype controls are represented by blue histograms, and detected markers are represented by red histograms. (D) Morphology of hUC-EVs observed by transmission electron microscopy (TEM). Scale bar: 100 nm. (E) Particle size distribution of hUC-EVs measured by nanoparticle tracking analysis (NTA). (F) Exosome markers (CD81, Alix, and Tsg101) and the endoplasmic reticulum protein Calnexin measured by western blotting. These experiments were repeated three times independently, and representative results are shown.

pyroptosis [28,52]. We hypothesized that hUC-EVs may protect chondrocytes and articular cartilage by inhibiting NLRP3-mediated cell pyroptosis and inflammatory cascade in OA rat models. In order to determine potential miRNA targets NLRP3, we used the website http://www.targetscan.org. And miR-223, which could directly target the 3′UTR of NLRP3 mRNA, decrease NLRP3 expression [53,54], was found to be significantly upregulated in cartilage treated with hUC-EVs (Fig. 4B). Then we examined the expression of miR-223 among chondrocytes treated with hUC-EVs or PBS using qRT-PCR, which confirmed that miR-223 level was significantly elevated in the EVs-treated chondrocytes (Fig. 4C). The probable binding site between NLRP3 mRNA and miR-223 was predicted (Fig. 4D). To verify the direct interaction between NLRP3 and miR-223, we built luciferase reporting vectors containing the wild type (WT) and mutant type (MUT) of 3′UTR sequence in NLRP3 mRNA and transfected the chondrocytes. As has been expected, the relative luciferase activity of the WT in the miR-223 mimics group was significantly reduced, while for the MUT there was no obvious change (Fig. 4E). Finally, the effect of hUC-EVs on NLRP3 protein expression levels was reconfirmed using western blotting. The protein level of NLRP3 and GSDMD distinctly decreased in chondrocytes cultured with hUC-EVs, which was partially reversed by miR-223 inhibitor, indicating the miR-223 dependence of above effects by hUC-EVs (Fig. 4F, quantification analysis is presented in Fig. S2). In conclusion, miR-223 was upregulated both in chondrocytes and cartilage tissues after hUC-EVs treatment, and it could directly target NLRP3 to mediate the inhibitory effect on NLRP3 expression.

2.5. CTP- and mir-engineering of hUC-EVs

Based on above findings, to further enhance the hUC-EVs' effect on anabolism promoting and inflammation inhibiting of chondrocyte and cartilage, and provide a promising therapeutic regimen for osteoarthritis treatment, two engineering methods were carried out to generate three kinds of engineered EVs (Fig. 5A). Three plasmids, encoding the Collagen II-targeting peptide (CTP)-lysosome-associated membrane glycoprotein 2 b (Lamp2b), enhanced green fluorescent protein (EGFP)-Lamp2b, or CTP-EGFP-Lamp2b were constructed and packaged with lentiviral vectors. The lentiviruses were then applied to transfect

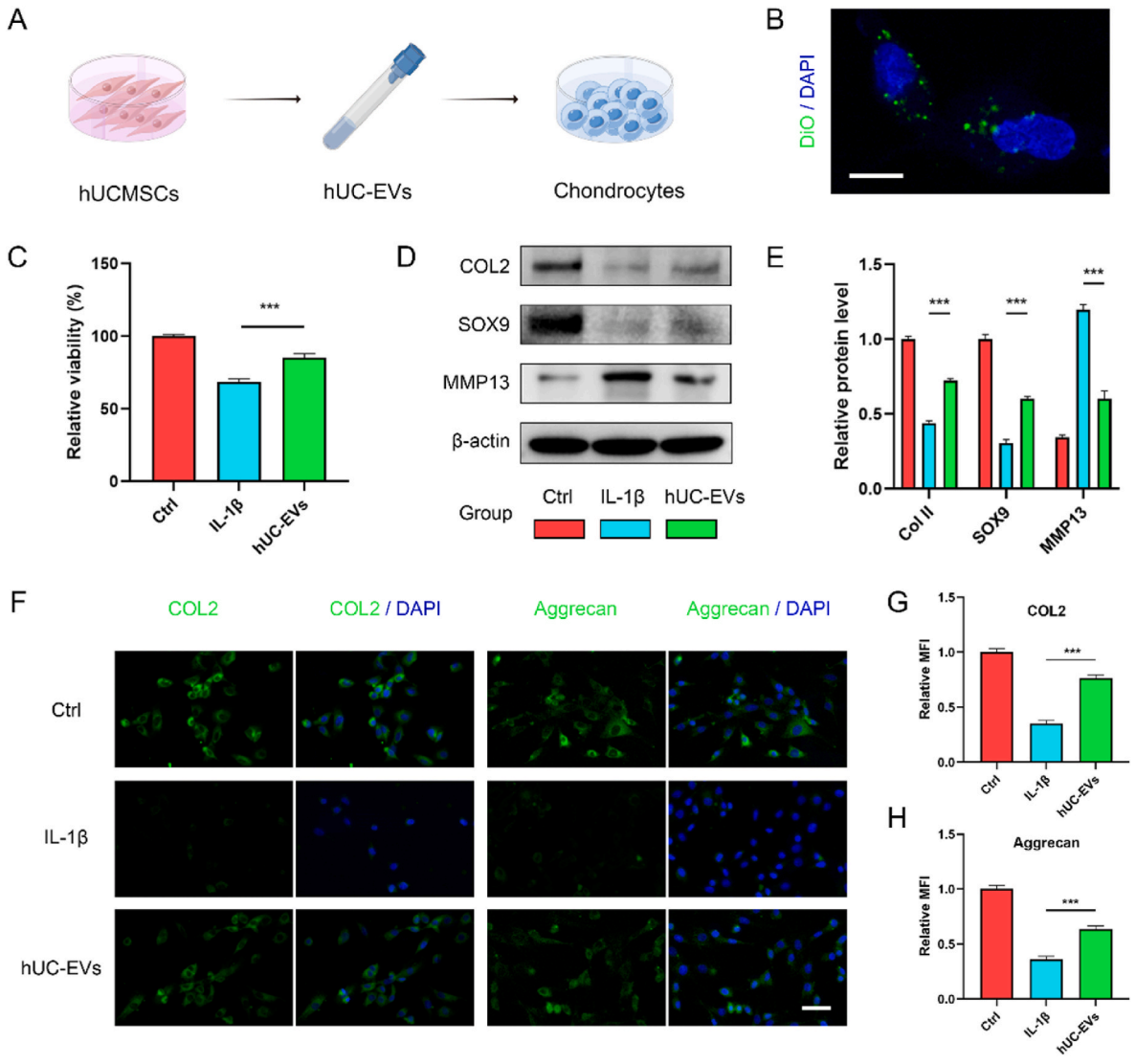

Fig. 2. HUC-EVs promote cell survival and anabolism of IL-1β-induced chondrocytes.
(A) Schematic of in vitro experiments. (B) Cellular uptake of DiO-labelled hUC-EVs by chondrocytes observed using confocal micrograph, scale bar: 10 μm. (C) Cell viability of chondrocytes measured using CCK-8 assays. (D–E) Protein levels of Collagen II, SOX9, and MMP13 in chondrocytes detected by western blotting. The color blocks correspond to the groups. (F–H) Collagen II and Aggrecan expressions in chondrocytes measured by immunofluorescence, scale bar: 50 μm. MFI: mean fluorescence intensity. ***P < 0.001. These experiments were repeated three times independently, and representative results are shown.

hUCMSCs to generate surface-modified EVs (Fig. 5B). The efficiency of the transfection in hUCMSCs was evaluated by fluorescence imaging, and more than 80% hUCMSCs transfected with lentivirus vectors are positive for EGFP, indicating that hUCMSCs with EGFP-Lamp2b or CTP-EGFP-Lamp2b expression were successfully established (Fig. 5C). Then, the CTP-EGFP-Lamp2b-EVs and EGFP-Lamp2b-EVs were injected into joint cavity of rat knees, and after 24 h, the fluorescence imaging indicated that CTP-EGFP- Lamp2b-EVs were mainly distributed in the articular cartilage, while a large proportion of EGFP-Lamp2b-EVs were absorbed by synovium, showing good cartilage-targeting ability of CTP-modified EVs (Fig. 5D, the quantification data is presented in Fig. S4A as the ratio of MFI in cartilage and synovium). After 48 h, fluorescence imaging confirmed that CTP-EGFP-Lamp2b-EVs entered knee chondrocytes more effectively than EGFP-Lamp2b-EVs (Figs. S3 and S4B). Then, miR-223 was loaded into the ordinary hUC-EVs and primarily-engineered CTP-EVs by electroporation, generating the miR-223-abundant Mir-EVs and dual-engineered CTP/Mir-EVs, respectively. The morphology of EVs remained intact after miR-223 electroporation, which was observed by TEM and dynamic light scattering (Fig. S5). We measured the miRNA loading efficiency, by comparing the free miR-223 left in the solution to the total input, and it turned out to be around 60% in either hUC-EVs or CTP-EVs (Fig. S6).

2.6. CTP- and mir-engineering both amplify the effect of hUC-EVs on promoting survival and improving anabolism of chondrocytes via mir-223/NLRP3/pyroptosis axis

We next observed the therapeutic effects of the various engineered EVs in vitro and validated our conjecture that the miR-223/NLRP3 axis mediated the beneficial effects of hUC-EVs and subsequent engineered EVs on chondrocyte protection. Briefly, we treated IL-1β-induced chondrocytes with aforesaid different EVs (Mir-EVs, CTP-EVs and CTP/Mir-EVs) at the concentration of 5×10^8 particles/ml for 24 h. In reverse validation experiment group, for activating NLRP3, the cells were treated with a NLRP3 agonist – nigericin sodium salt (NSS) (1 μM). The schematic is shown in Fig. 6A and experimental grouping in Fig. 6B.

To assess the effect of engineered EVs on cell viability and pyroptosis, CCK-8 assay (Fig. 6C), and LDH activity analysis of supernatant (Fig. 6D), which is used as a measure of pyroptosis were carried out. Mir-EVs and CTP-EVs could markedly reverse IL-1β-induced viability

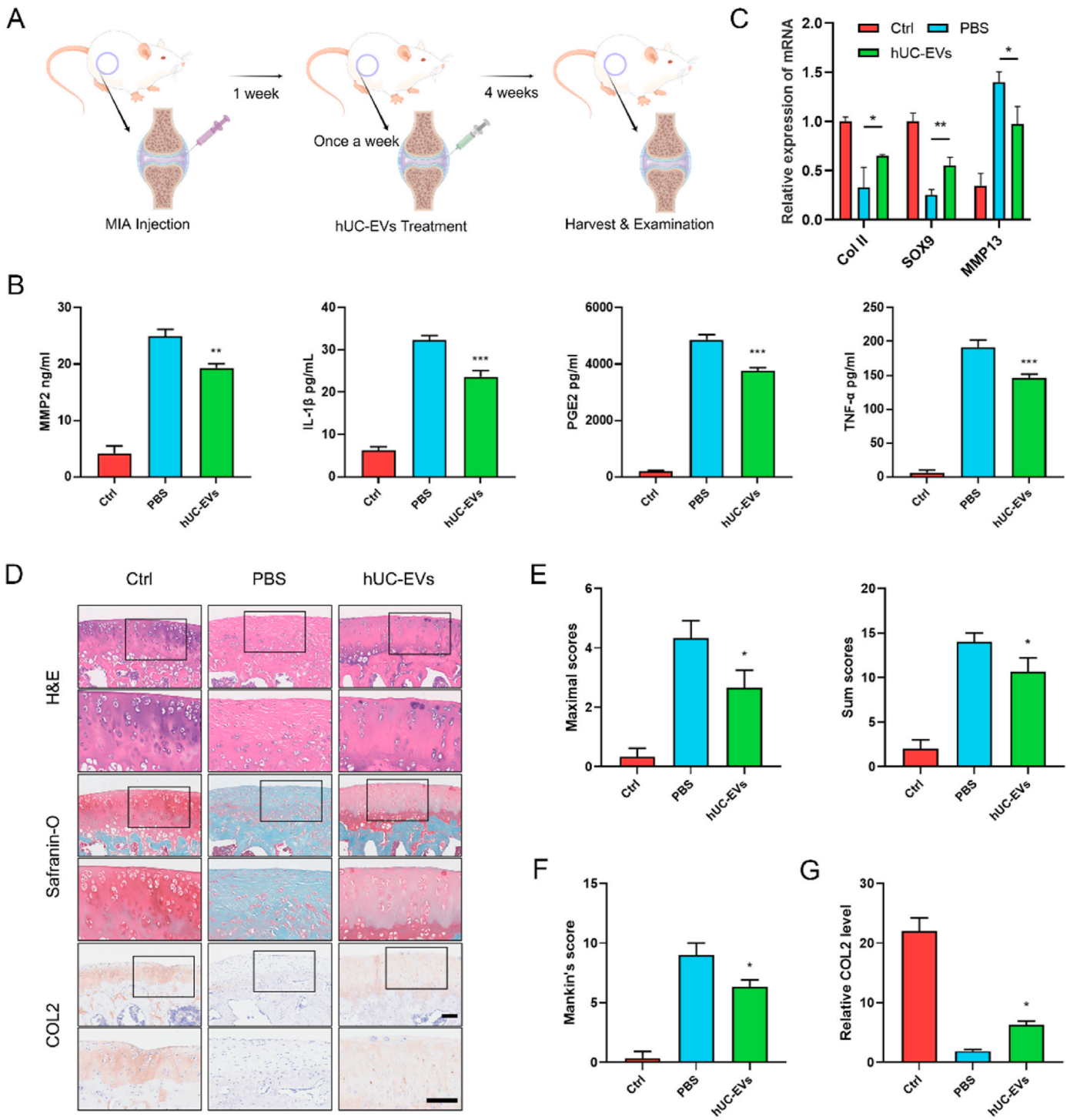

Fig. 3. HUC-EVs alleviate the inflammation and cartilage degeneration in OA rat model
(A) Schematic diagram of animal experiments. (B) ELISA analysis of pro-inflammatory factors (MMP-2, PGE2, IL-1β, and TNF-α) in OA models. (C) qRT-PCR analysis of anabolic factors (Collagen II, SOX9), and catabolic factor (MMP13) in cartilage samples. (D) H&E, Safranin O/Fast Green, and immunohistochemical staining of knee joint sections. Scale bar: 100 μm. Cartilage degradation evaluated by (E) the OARSI scoring system and (F) Mankin's score. (G) Semi-quantitative analysis of Collagen II expression in immunohistochemical staining. n = 3 for each group. *P < 0.05; **P < 0.01; ***P < 0.001 compared with the PBS group.

decrease of chondrocytes, along with the LDH release, and no significant difference was observed between the two groups. The dual-engineered CTP/Mir-EVs improved the viability and downregulated the LDH level further, which showed significant differences compared with Mir-EVs and CTP-EVs. Interestingly, the gain effects of all engineered EVs were reversed by NSS, which proved that engineered EVs exert their protective roles via miR-223/NLRP3/pyroptosis axis. The protein levels of Collagen II, SOX9, MMP13, NLRP3 inflammasome and pyroptosis-related molecules (NLRP3, cleaved caspase-1, GSDMD-N) was measured by western blotting (Fig. 6E and F). Accordingly, Mir-EVs and CTP-EVs treatment significantly increased Collagen II and SOX9 expression, while downregulated the protein level of MMP13, NLRP3, cleaved caspase-1, and GSDMD-N. CTP/Mir-EVs further enhanced these effects and NSS reversed the above. The results of immunofluorescence

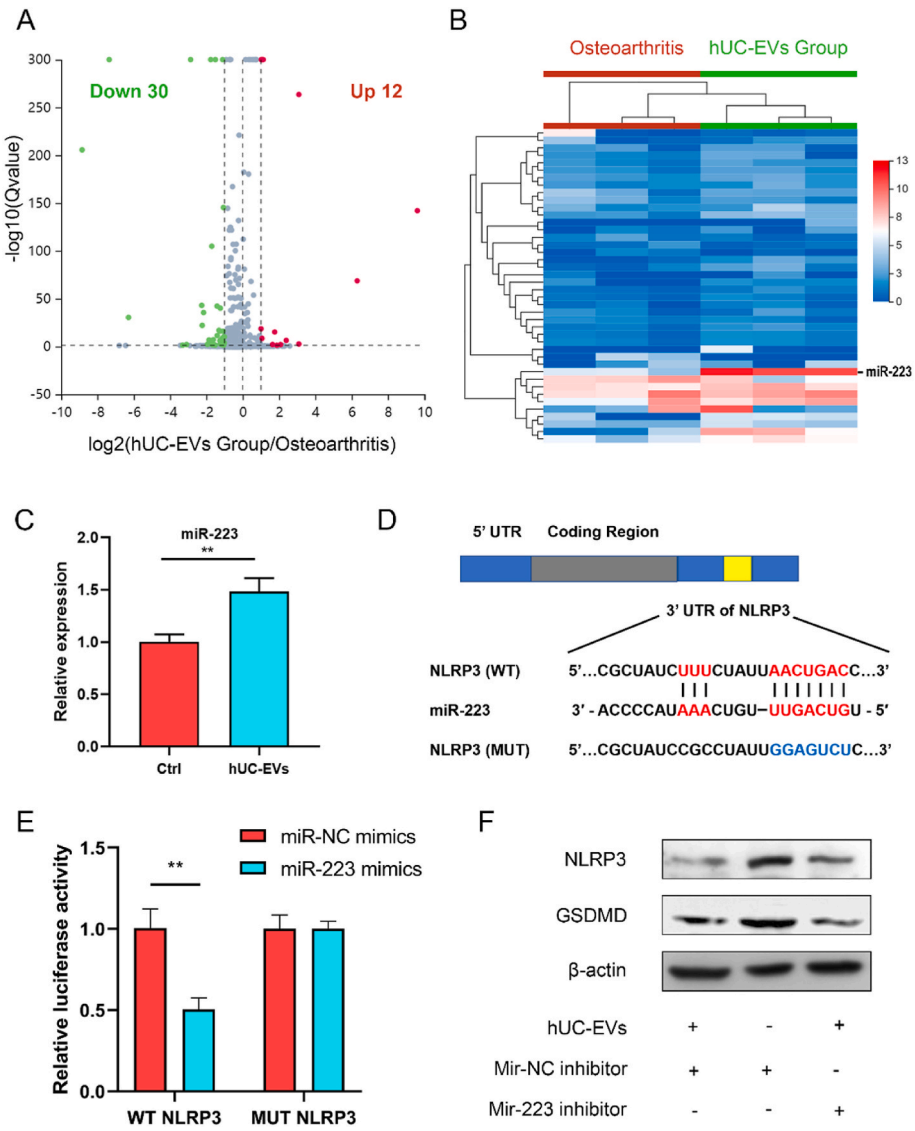

Fig. 4. miR-223 mediates the inhibitory effect of hUC-EVs on NLRP3
(A) Volcano plot illustrating miR expression of OA rat knee joint cartilage treated with or without hUC-EVs. Red dots, up-regulated miRs, blue dots, down-regulated miRs, gray dots, miRs with no significant difference. (B) Heat map of miRNA sequencing (miRNA-seq) analysis. Red arrow: miR-223. (Red: high expression, blue: low expression, n = 3 per group) (C) qRT-PCR analysis of miR-223 (n = 3 per group). (D) Binding seq of NLRP3 and miR-223. (E) Dual-luciferase reporter gene assay validating the interaction between NLRP3 and miR-223. (F) Protein levels of NLRP3 examined by western blotting. **P < 0.01. These experiments were repeated three times independently, and representative results are shown.

staining also supported the findings (Fig. 6G-L). In summary, the above results showed that CTP- and Mir-engineering both amplify the effect of hUC-EVs on promoting survival and improving anabolism of chondrocytes via mir-223/NLRP/pyroptosis axis, and the dual-engineered CTP/Mir-EVs achieved better therapeutic results than single modified Mir-EVs or CTP-EVs.

2.7. Dual-engineered CTP/Mir-EVs further promote cartilage repair, inhibit inflammation and ameliorate the severity of OA

Finally, we validated that the newly engineered EVs could further promote cartilage repair and ameliorate the severity of OA in rat model and provide as a novel and rewarding therapeutic choice for clinical osteoarthritis treatment.

The MIA-induced OA rat were treated with the newly engineered EVs (diluted in PBS) or negative control (PBS) once a week for 4 times 1 week after the MIA injection. The knee joints were harvested and examined at 5 weeks. In order to observe the activation of inflammasomes more directly and objectively, IF staining of NLRP3 and GSDMD-N in articular cartilage sections was performed (Fig. 7A), and the semiquantitative analysis was in Fig. S7. The results validated that hUC-EVs decreased the number of chondrocytes positive for NLRP3 and GSDMD-N in the cartilage, inhibiting the NLRP3 inflammasome activation and pyroptosis in OA knees, and engineered EVs amplified this effect, among which the CTP/Mir-EVs performed the best. To verify the anti-inflammatory effects of the engineered EVs, pro-inflammatory factors in cartilage samples were measured by ELISA, which suggested that CTP/Mir-EVs markedly reduced the generation of MMP2, IL-1β, TNF-α, and PGE2 in vivo compared with Mir-EVs and CTP-EVs (Fig. 7B). Consistent with the above results, H&E, Safranin O/Fast Green, and immunohistochemical staining (collagen II, collagen I) of knee joint sections showed that Mir-EVs and CTP-Mirs both partly reversed the changes of OA, while CTP/Mir-EVs further restored nearly normal articular cartilage structure (Fig. 7C, Fig. S8A). The CTP/Mir-EVs group had the lowest maximal and summed scores of the OARSI (Fig. 7D), along with the Mankin's score (Fig. 7E). Moreover, collagen II and collagen I protein levels in articular cartilage were also the highest and the lowest in the CTP/Mir-EVs group, respectively (Fig. 7F, Fig. S8B). Micro-CT was performed to investigate the progressive cartilage damage and subchondral bone degeneration, which usually shows joint space narrowing and bone volume/total volume (BV/TV) decreasing [55]. The results revealed that the joint space widths (JSWs) significantly decreased in the PBS group compared with the control group, the EVs, especially the CTP/Mir-EVs treatment significantly increased the JSW (Fig. 8 A, C, and D). Also, the subchondral bone was obviously destroyed, with the BV/TV declined in the PBS group, and CTP/Mir-EVs significantly suppressed this effect,

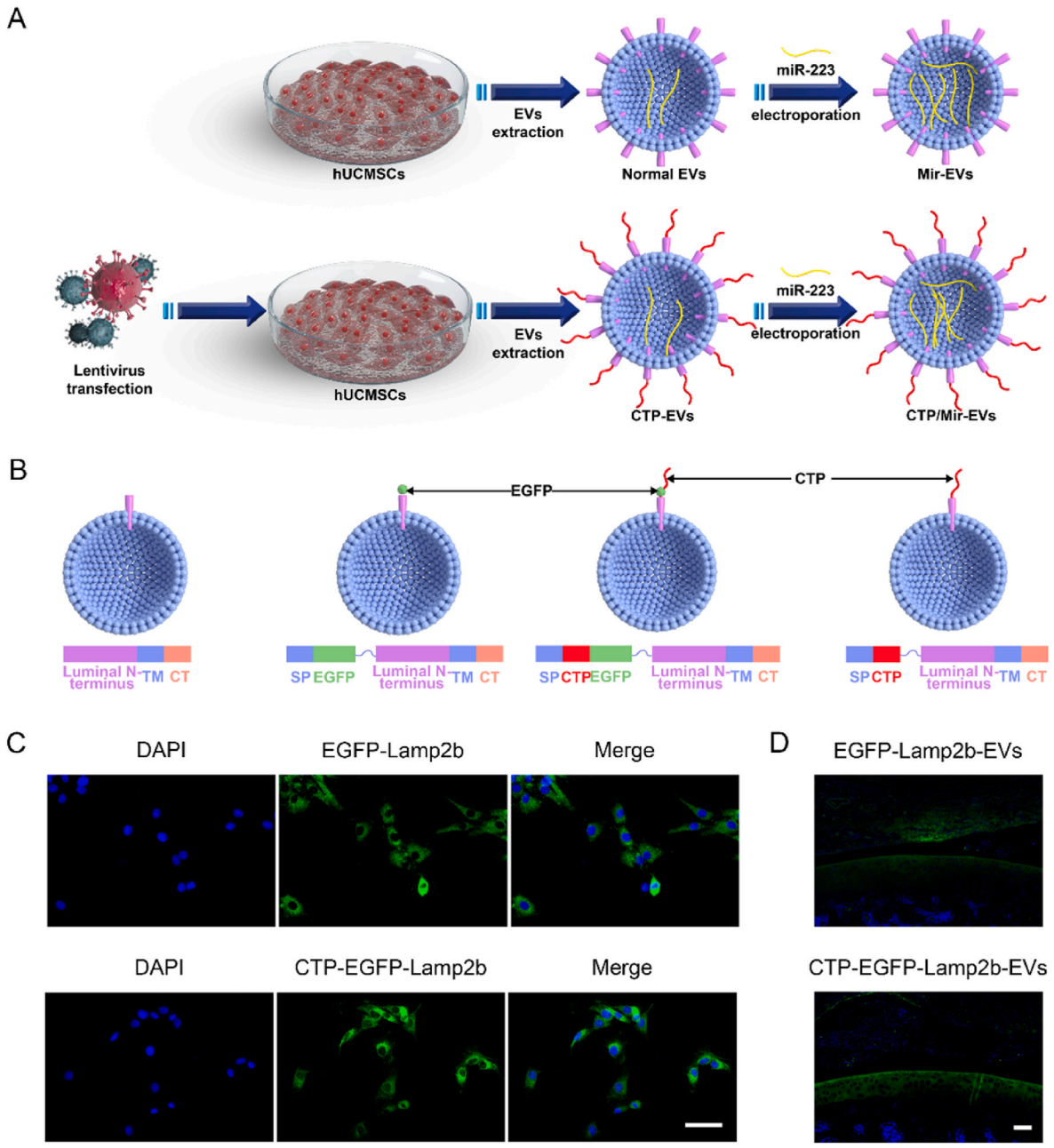

Fig. 5. CTP- and Mir-engineering of hUC-EVs
(A) Schematic diagram of EVs engineering (CTP modifying and miR-223 loading). (B) Schematic of the plasmid constructs. SP, signal peptide; TM, transmembrane domain; CT, C terminus. (C) Overexpression of EGFP-lamp2b or CTP-EGFP-lamp2b in hUCMSCs observed using fluorescence imaging. Scale bar = 50 μm. (D) Cartilage-targeting ability of CTP-modified EVs in rat knees observed using fluorescence imaging. Scale bar = 100 μm. These experiments were repeated three times independently, and representative results are shown.

indicating that CTP/Mir-EVs can alleviate joint damage effectively (Fig. 8B, E). Collectively, the above results showed that CTP/Mir-EVs could further inhibit NLRP3 inflammasome activation, chondrocyte pyroptosis and cartilage degradation, which amplified the therapeutic effect for MIA-induced OA.

A schematic overview of the proposed underlying mechanism of our dual-engineered CTP/Mir-EVs in promotion of cartilage repair was concluded and presented as Scheme 1.

3. Conclusion

In this study, we demonstrated the therapeutic effects of human umbilical cord MSC-derived extracellular vesicles (hUC-EVs) on OA, and revealed an underlying mechanism. We successfully isolated EVs from hUCMSCs, which alleviated the OA severity in vivo, and inhibited cell death, enhanced anabolism of chondrocytes in vitro. MiRNA sequencing showed that the expression of miR-223, which could negatively regulate NLRP3 was significantly increased in the cartilage of exosome-treated knees. Subsequent experiments proved that miR-223 directly targets NLRP3 to mediate the protective effects of hUC-EVs on chondrocytes survival and cartilage repair. Then, exogenous miR-223 was loaded into hUC-EVs by electroporation, and the collagen II-targeting peptide (WYRGRL) was modified onto the surface of hUC-EVs to obtain engineered hUC-EVs. The dual-engineered CTP/Mir-EVs enhanced the gain effects of hUC-EVs on OA treatment both in vivo and in vitro, and this can be reversed by NSS, a NLRP3 agonist. In brief, hUC-EVs maintain

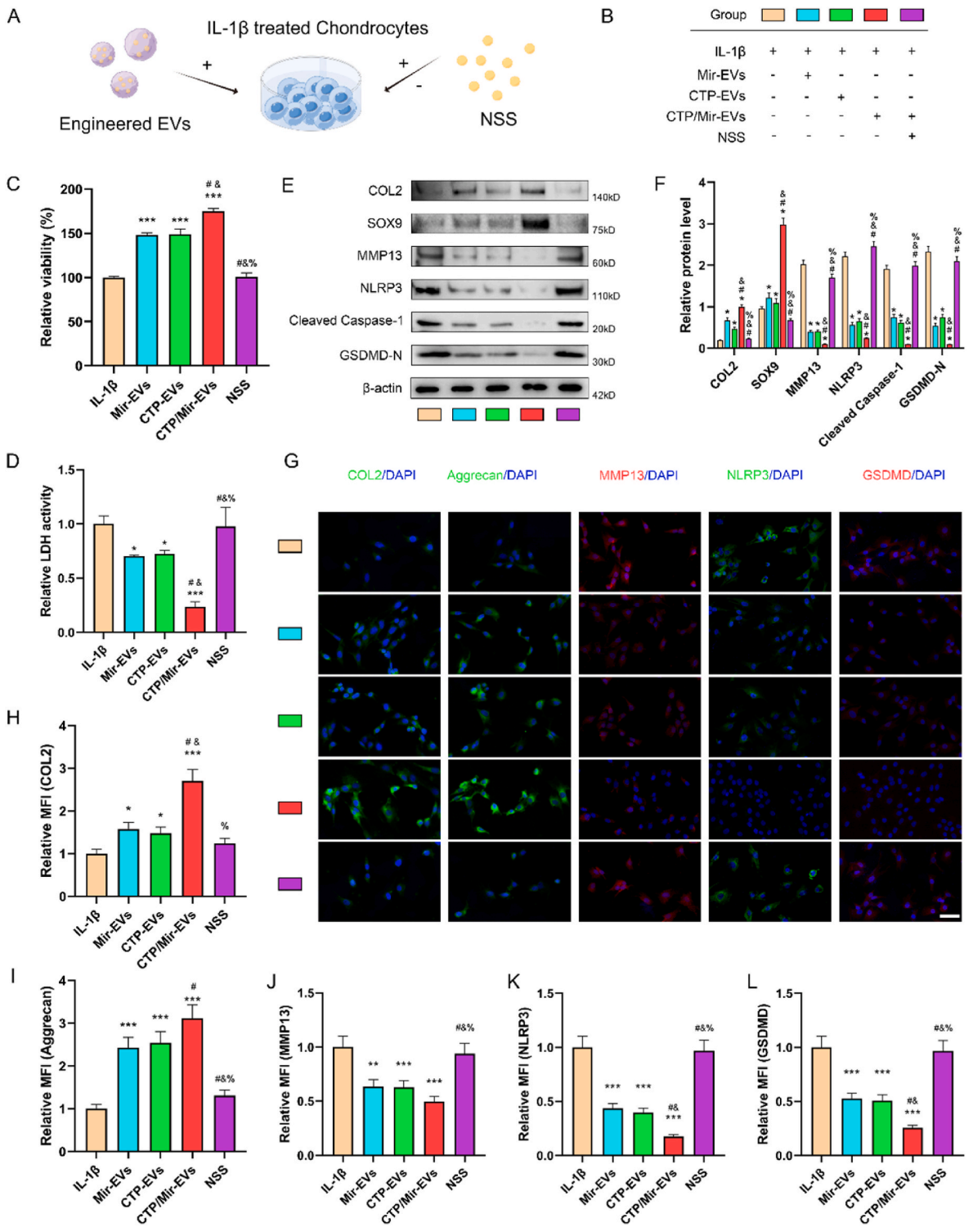

Fig. 6. CTP- and Mir-engineering both amplify the effect of hUC-EVs on promoting survival and improving anabolism of chondrocytes via miR-223/NLRP3/pyroptosis axis

(A) Schematic and (B) grouping of in vitro experiments, the color blocks correspond to the groups throughout this figure. (C) Cell viability of chondrocytes measured by CCK-8 assays. (D) LDH activity analysis of chondrocyte supernatant by its assay kit. (*E*–F) Protein expression levels of Collagen II, SOX9, MMP13, NLRP3 inflammasome-related molecules (NLRP3, cleaved caspase-1, and GSDMD-N) in chondrocytes measured by western blotting and the grayscale scanning analysis. (G–L) Detection of Collagen II, Aggrecan, MMP13, NLRP3, and GSDMD-N expressions in chondrocytes by immunofluorescence. Scale bar: 50 μm. MFI: mean fluorescence intensity. *P < 0.05, **P < 0.01, ***P < 0.001 compared with IL-1β group. #P < 0.05 compared with Mir-EVs group. &P < 0.05 compared with CTP-EVs group. %P < 0.05 compared with CTP/Mir-EVs group. These experiments were repeated three times independently, and representative results are shown.

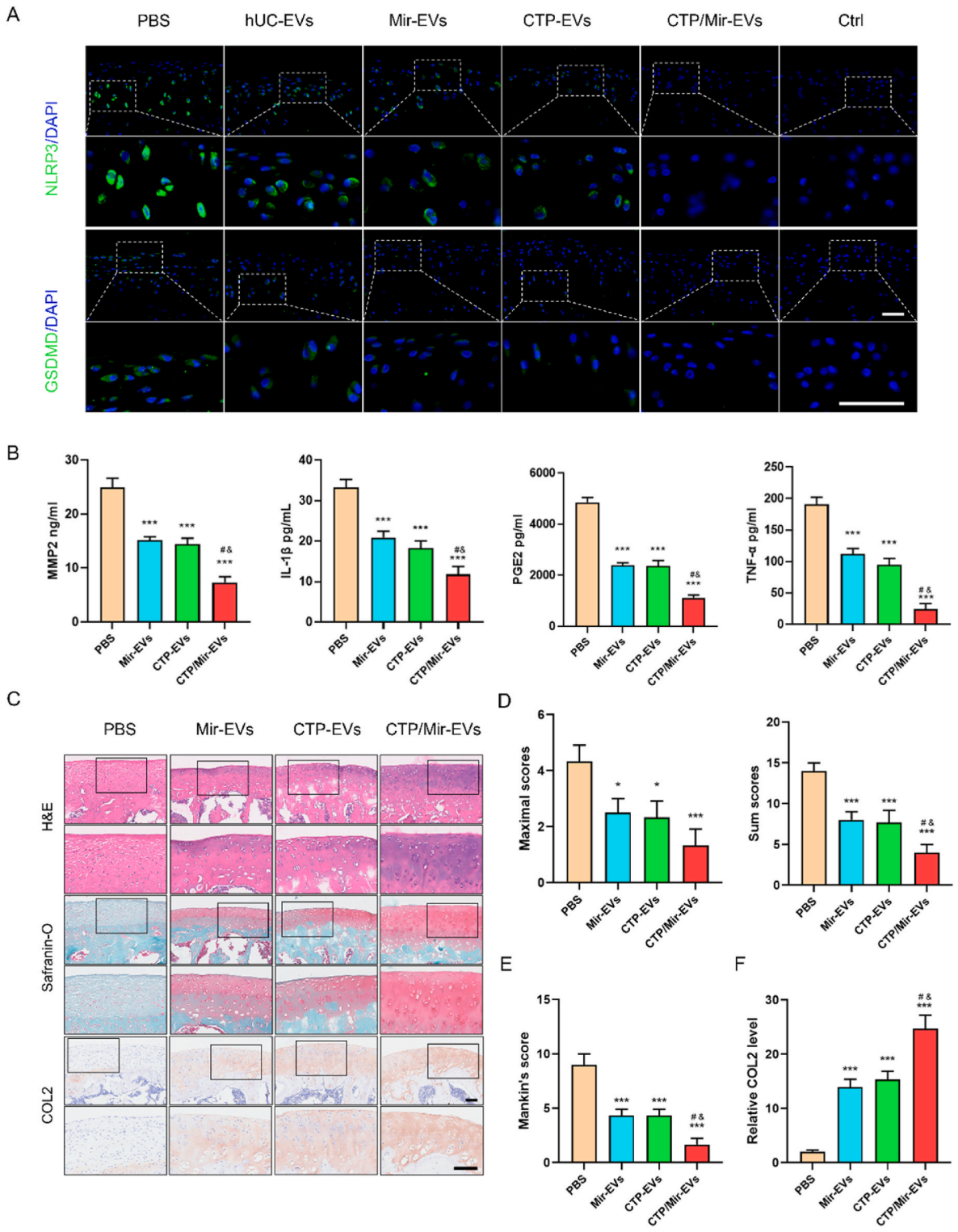

Fig. 7. Dual-engineered CTP/Mir-EVs further promote cartilage repair, inhibit inflammation and ameliorate the severity of OA.
(A) Immunofluorescence analysis of NLRP3 and GSDMD-N expressions in sections of knee joints. Scale bar: 50 μm. (B) ELISA analysis of pro-inflammatory factors in OA models, including IL-1β, MMP-2, TNF-α, and PGE2. (C) H&E, Safranin O/Fast Green, and IHC staining (Collagen II) of knee joint sections. Scale bar: 100 μm. Cartilage degradation evaluated by (D) the OARSI scoring system and (E) Mankin's score. (F) Semi-quantitative analysis of Collagen II expression in IHC staining. n = 3 for each group. *P < 0.05, ***P < 0.001 compared with PBS group. #P < 0.05 compared with Mir-EVs group. &P < 0.05 compared with CTP-EVs group.

chondrocyte homeostasis and protect articular cartilage from damage in OA rat via miR-223/NLRP3/pyroptosis axis. Engineered hUC-EVs overexpressing miR-223 and modified by cartilage-targeting peptide show an amplified therapeutic effect. As umbilical cords provide excellent sources of MSCs, hUC-EVs and such engineered EVs hold potential as future therapeutic strategies for OA.

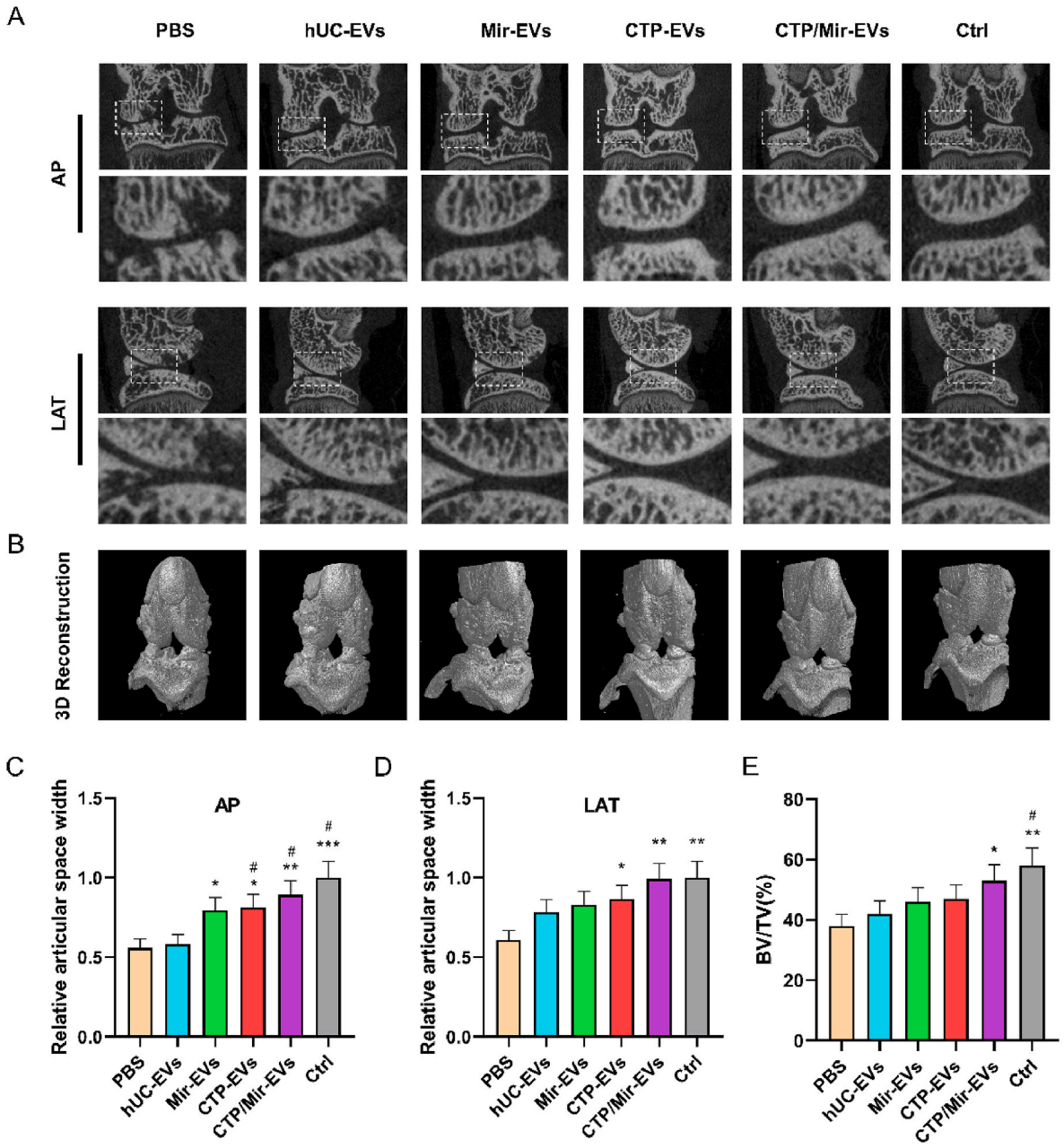

Fig. 8. Micro-CT demonstrating engineered CTP/Mir-EVs significantly delay the progression of knee OA.
(A) Sectional micro-CT images showing the knee joint in an anterior-posterior and lateral view. (B) Three-dimensional reconstruction of the knee joint. (C) The relative joint space widths measured from anterior-posterior images. (D) The relative joint space widths measured from lateral images. (E) The relative bone volume fraction (BV/TV) measured from three-dimensional reconstruction. n = 3 for each group. *P < 0.05, **P < 0.01, ***P < 0.001 compared with PBS group. #P < 0.05 compared with hUC-EVs group.

4. Experimental section

4.1. Cell preparation and identification

hUCMSCs were bought from Oricell™ (Cyagen Biosciences, China) and cultured in α-MEM medium (Hyclone, USA), supplemented with 10% fetal bovine serum (FBS; Gibco, USA) and 100 units/mL penicillin/streptomycin (1% P/S; Servicebio, China) in an incubator with 5% CO_2 at 37 °C. Passage 4 hUCMSCs were seeded in six-well plates switched to osteogenic, adipogenic, or chondrogenic differentiation medium (Oricell™, Cyagen Biosciences) for 3 weeks. Alcian Blue, Oil Red O, and Alizarin Red S staining were performed according to standard protocols using Alcian Blue 8GX (Sigma), Oil Red O (Sigma), and Alizarin Red S (Sigma), respectively, to confirm their multiple differentiation potential. Surface protein markers of hUCMSCs were detected using flow cytometry with monoclonal antibodies (ThermoFisher, USA).

For extracting chondrocytes, the articular cartilage of Sprague-Dawley rats (male, 5 days old) was processed as previously described [56]. In brief, the cartilage was diced and digested with 0.2% type II collagenase (Sigma, USA) in DMEM/F12 (Invitrogen, USA) solution at 37 °C for 6 h. Then, the cell suspension was filtered, and chondrocytes were obtained. The chondrocytes were cultured with DMEM/F12 medium supplemented with 10% FBS and 1% P/S which was exchanged every other day. The chondrocytes were not passed over three generations to prevent phenotypic loss and dedifferentiation.

4.2. Isolation and characterization of hUC-EVs

Cells were washed twice with PBS after reaching 80% confluency, and then cultured with medium supplemented with 10% exosome-depleted FBS (SBI, USA) and 1% P/S. We collected conditioned medium from hUCMSCs after two days to isolate EVs. EVs were extracted by ultracentrifugation, as previously described [57]. Briefly, the conditioned medium was centrifuged at 300 g for 10 min, 2000 g for 20 min and then at 10000 g for 30 min at 4 °C, which allowed the remaining cells and debris to be clearly removed. The supernatant was then ultracentrifuged at 100,000 g for 70 min twice at 4 °C, the pellet (EVs) was resuspended in 50 μL PBS. We stored hUC-EVs at −80 °C until further use. We used a NanoSight LM10 instrument (Malvern, UK) to measure EV concentration and size distribution. To determine the morphology of hUC-EVs, transmission electron microscopy (TEM) was used (Hitachi H7500, Japan). The surface markers of hUC-EVs were analyzed by western blotting (antibodies purchased from Proteintech, China).

4.3. Lentivirus construction and transfection

The CTP-(EGFP-)Lamp2b expressing lentiviral vector was custom designed on VectorBuilder (Chicago, IL, USA) and obtained from Yunzhou Co, LTD (Guangzhou, China). hUCMSCs were seeded in six-well culture plates at a density of 3×10^5 cells per well and allowed to adhere for 24 h in a humidified incubator with 5% CO_2 before transduction. Following the manufacturer's instructions, cells were transduced with 1 mL of media containing the appropriate virus at a MOI of 10. We generated stable over-expression hUCMSC lines after a 3-day antibiotic selection with puromycin. A fluorescence microscope was used to visualize and count EGFP-positive cells during selection to confirm transduction efficiency. To collect engineered CTP-EVs, stable cell lines were seeded in a 10 cm dish at a density of 5×10^6.

4.4. miRNA loading by electroporation

An electroporation buffer containing 1.15 mM potassium phosphate, pH = 7.2, 25 mM potassium chloride, and 21% Optiprep was used to mix 0.5 μmol miR-223 mimics with 10 μg of total EVs. Using a Gene Pulser II system (BioRad Laboratories, CA), the mixture was electroporated in a 4 mm electroporation cuvette for 30 min at 350 V and 150 μF, and then incubated at 37 °C for 30 min to assure the membrane recovery of the EVs. Ultracentrifugation at 120,000×*g* and 4 °C for 70 min removed free unloaded miR-223, and the final pellet (EVs) was resuspended in PBS and stored at −80 °C. Using a fluorimeter that excited at 532 nm and emitted at 580 nm, the loading efficiency was calculated as follows: miRNA loading efficiency = (encapsulated miRNA/initial input of miRNA) *100%.

4.5. Chondrocyte treatment

To estimate the effect of EVs on chondrocyte viability and metabolism, chondrocytes were treated with the various EVs (5×10^8 particles/ml) in the presence or absence of IL-1β (10 ng/mL) for 24 h, in which IL-1β was used to simulate the microenvironment of OA in vitro [44].

4.6. Cell viability test

CCK-8 (Dojindo, Kumamoto, Japan) was used to evaluate chondrocyte viability. We cultured the chondrocytes for 12 h in a 96-well plate (2000 per well). A complete medium containing different EVs was added to each well. Following further incubation for 24 h, each well was washed three times with complete medium. Each well was then added 100 μL of complete medium containing 10% CCK-8 reagent and the absorbance at 490 nm was measured by a microplate reader (Bio-Rad, US) after 4 h of incubation.

4.7. Western blot analysis

A BCA protein assay kit (Beyotime, China) was used to measure protein concentrations in cell lysates harvested using RIPA (Beyotime, China). The Western blot analysis was performed as described previously [58]. Anti-collagen II (Abcam, ab34712), anti-Sox9 (Abcam, ab185966), *anti*-MMP13 (Abcam, ab39012), *anti*-NLRP3 (Abclonal, A5652), *anti*-caspase-1 (Abclonal, A0964), *anti*-GSDMD-N (Abclonal, A20197) were used as primary antibodies.

4.8. Quantitative RT-PCR analysis

TRIzol Reagent (Invitrogen, America) was used to extract total RNA for mRNA detection. PrimeScript™ RT reagent Kit with gDNA Eraser (Takara, Japan) was used to generate complementary DNA templates. MiRNAs were isolated using the miRNA Isolation Kit (BioFlux, Japan) for detection. RT-PCR was performed using SYBR Premix Ex Taq™ II Kit (Takara, Japan) on Mx3000 P system (Stratagene, America), with each sample prepared in triplicate as recommended by the manufacturer. An All-in-One™ miRNA Fist-Strand cDNA Synthesis Kit and an All-in-One™ miRNA qPCR Kit (GeneCopoeia, America) were used for RT-PCR. RNA expression levels were calculated using the $2^{-\Delta\Delta CT}$ method. Table S1 lists the primers used for RT-PCR.

4.9. Immunofluorescent staining in vitro

To evaluate the expression of collagen II, aggrecan, MMP13, NLRP3, and GSDMD, the chondrocytes were sequentially stained with anti-collagen II (Abcam, ab34712), *anti*-aggrecan (Abcam, ab3778), *anti*-MMP13 (Abcam, ab39012), *anti*-NLRP3 (Abclonal, A5652), and *anti*-GSDMD-N (Abclonal, A20197), then secondary antibodies, respectively. Nuclei were stained with DAPI (Thermo Fisher Scientific).

4.10. Induction of osteoarthritis and Intra-articular injection of EVs

Study design and animal experiments were approved by the Ethics Committee of Shanghai Sixth People's Hospital (Animal Welfare Ethics No: DWLL2022-0594). The OA model was established using SD rats (8 weeks, 200–250 g) purchased from Shanghai Sixth People's Hospital. Sodium pentobarbital at 0.5% was injected intraperitoneally (0.9 mL/100 g) for general anesthesia. Through the infrapatellar ligament, 50 μL MIA (Sigma-Aldrich) at 20 mg/mL was injected intraarticularly to induce OA. Intra-articular injections of 50 μL PBS or 50 μL EV (10^{10} particles/ml) for 4 weeks (once a week) 1 week after the MIA injection were administered to rats.

4.11. Specimen preparation and histopathology analysis

Rats were sacrificed 5 weeks after MIA injection by anesthetic overdose. We fixed the knee joints in 4% paraformaldehyde, decalcified them in 20% formic acid, and embedded them in paraffin. At 50-mm intervals, serial sagittal sections were taken including the entire joint. Safranin O/Fast green, HE, immunohistochemical, and immunofluorescent stainings were performed on the sections. Matrix proteoglycan and overall joint morphology were assessed by Safranin O/Fast green-staining. Osteoarthritis Research Society International (OARSI) scoring system [59], along with the Mankin's score [60] were used to evaluate the grading of OA progress and cartilage degeneration of every sample in each group. Anti-collagen II antibody (Abcam, ab34712), *anti*-NLRP3 (Abclonal, A5652), and *anti*-GSDMD-N (Abclonal, A20197), were used as primary antibodies for IHC and IF, respectively.

4.12. ELISA analysis

The supernatant of chondrocytes in different groups was harvested for ELISA to evaluate the level of LDH (Cloud-Clone, USA). The cartilage tissues were also harvested and homogenized in PBS (1 mL). After centrifugation at 10,000×*g* for 15 min at 4 °C, the supernatants were used for detecting the expression of IL-1β (Enzolife, ADI-900-131 A), MMP2 (Raybiotech, ELR-MMP2-1), TNF-α (Enzolife, ADI-900-086 A), and PGE-2 (Cayman, 514,010) by the corresponding ELISA kits. Microplate readers (Bio-Rad, USA) were used to measure the absorbance at 450 nm.

4.13. Micro-computed tomography imaging

A high-resolution micro-CT scanner Skyscan 1176 (Bruker, Kontich, Belgium) was used to examine the knee joints of each rat.

4.14. MiRNA sequencing and analysis

Total RNA from cartilage was extracted for miRNA sequencing (miRNA-seq). Library preparation and miRNA-seq were performed by BGI (Shenzhen, China). To prepare the library, small RNAs ranging from 18 to 30 nucleotides (nt) were fractionated from the total cartilage RNA. A HiSeq 2500 platform (Illumina, San Diego, CA, USA) was used to sequence the PCR products.

4.15. Dual-luciferase reporter assay

A dual-luciferase miRNA target expression vector (GP-miRGLO, GenePharma, Shanghai, China) was cloned from the 3′UTR region of NLRP3 mRNA containing the miR-223 binding site, wild or mutant (AACUGAC mutated to GGAGUCU). MiR-223 mimics and mimic NC were co-transfected into HEK293T cells with wild and mutant vectors. A Dual-luciferase Reporter Assay (Promega, Madison, WI, USA) was performed to measure the Firefly and Renilla luciferase activities.

4.16. Statistical analysis

Numerical data are presented as mean ± standard deviation (SD). All statistical analyses in this study were performed using SPSS 26.0 software (IBM Corp., Armonk, NY, USA). In the figure legend, the sample size (n) for each statistical analysis is indicated. One-way ANOVA with Tukey post hoc analysis was used to compare the mean values among groups. The level of significance was set at $\alpha = 0.05$ (two-tailed).

Declaration of competing interest

The authors declare that there are no conflicts of interest.

CRediT authorship contribution statement

Weixuan Liu: Conceptualization, Methodology, Investigation, Writing – original draft. **Anqi Liu:** Formal analysis, Methodology, Writing – original draft. **Xujun Li:** Investigation, Methodology, Writing – original draft. **Ziyang Sun:** Formal analysis. **Zhenghua Sun:** Formal analysis. **Yaru Liu:** Resources. **Gang Wang:** Validation. **Dan Huang:** Resources. **Hao Xiong:** Conceptualization, Writing – review & editing. **Shiyang Yu:** Project administration, Supervision. **Xintao Zhang:** Writing – review & editing, Supervision. **Cunyi Fan:** Writing – review & editing, Project administration, Funding acquisition.

Acknowledgements

W.L., A.L. and X.L. contributed equally to this work. This work is financially supported by the Key Project of National Natural Science Foundation of China (81830076), the National Natural Science Foundation of China (82272568), the Shanghai Engineering Technology Research Center and Professional Technology Service Platform project of 2020 “Science and Technology Innovation Action Plan” of Shanghai (20DZ2254100), and the Biomedical Technology Support Special Project of Shanghai 2021 “Science and Technology Innovation Action Plan” (21S31902300).

Appendix A. Supplementary data

Supplementary data to this article can be found online at https://doi.org/10.1016/j.bioactmat.2023.06.012.

Abbreviations List

NLRP3	NOD-like receptor family, pyrin domain containing 3
OA	Osteoarthritis
MSCs	mesenchymal stem cells
EVs	extracellular vesicles
hUCMSCs	human umbilical cord mesenchymal stem cells
hUC-EVs	extracellular vesicles derived from human umbilical cord mesenchymal stem cells
3′UTR	3′ untranslated region
IL-1β	interleukin-1β
IL-18	interleukin-18
GSDMD	gasdermin D
CTP	collagen II-targeting peptides
TEM	Transmission electron microscopy
NTA	Nanoparticle Tracking Analysis
CCK-8	cell counting kit-8
COL2	Collagen II
MMP13	matrix metalloproteinase 13
MMP2	matrix metalloproteinase 2
SOX9	SRY (sex determining region Y)-box 9
MIA	monosodium iodoacetate
TNF-α	tumor necrosis factor α
PGE2	prostaglandins E2
ECM	extracellular matrix
OARSI	the Osteoarthritis Research Society International (OARSI) scoring system
H&E	Hematoxylin-eosin
qRT-PCR	Quantitative real-time polymerase chain reaction
EGFP	enhanced green fluorescent protein
Lamp2b	lysosome-associated membrane glycoprotein 2 b
ELISA	Enzyme-linked immunosorbent assay
LDH	Lactate Dehydrogenase
NSS	nigericin sodium salt
JSWs	joint space widths
BV/TV	bone volume/total volume

References

[1] D.J. Hunter, S. Bierma-Zeinstra, Osteoarthritis, Lancet 393 (10182) (2019) 1745–1759.
[2] D. Prieto-Alhambra, A. Judge, M.K. Javaid, C. Cooper, A. Diez-Perez, N.K. Arden, Incidence and risk factors for clinically diagnosed knee, hip and hand osteoarthritis: influences of age, gender and osteoarthritis affecting other joints, Ann. Rheum. Dis. 73 (9) (2014) 1659–1664.
[3] J. Clarke, Bone stresses out cartilage in OA, Nat. Rev. Rheumatol. 17 (5) (2021) 250.
[4] M. Varela-Eirin, J. Loureiro, E. Fonseca, S. Corrochano, J.R. Caeiro, M. Collado, M. D. Mayan, Cartilage regeneration and ageing: targeting cellular plasticity in osteoarthritis, Ageing Res. Rev. 42 (2018) 56–71.
[5] E.M. Roos, N.K. Arden, Strategies for the prevention of knee osteoarthritis, Nat. Rev. Rheumatol. 12 (2) (2016) 92–101.
[6] C.R. Harrell, B.S. Markovic, C. Fellabaum, A. Arsenijevic, V. Volarevic, Mesenchymal stem cell-based therapy of osteoarthritis: current knowledge and future perspectives, Biomed. Pharmacother. 109 (2019) 2318–2326.
[7] L. Kong, L.Z. Zheng, L. Qin, K.K.W. Ho, Role of mesenchymal stem cells in osteoarthritis treatment, J Orthop Translat 9 (2017) 89–103.

[8] M. Zhao, S. Liu, C. Wang, Y. Wang, M. Wan, F. Liu, M. Gong, Y. Yuan, Y. Chen, J. Cheng, Y. Lu, J. Liu, Mesenchymal stem cell-derived extracellular vesicles attenuate mitochondrial damage and inflammation by stabilizing mitochondrial DNA, ACS Nano 15 (1) (2021) 1519–1538.

[9] J.Lee Han, W.S. Kim, J.S. Choi, S. Yang, J.H. Park, D.G. Jo, Y.W. Cho, Small extracellular vesicles from human adipose-derived stem cells attenuate cartilage degeneration, J. Extracell. Vesicles 9 (1) (2020), 1735249.

[10] E. Mianehsaz, H.R. Mirzaei, M. Mahjoubin-Tehran, A. Rezaee, R. Sahebnasagh, M. H. Pourhanifeh, H. Mirzaei, M.R. Hamblin, Mesenchymal stem cell-derived exosomes: a new therapeutic approach to osteoarthritis? Stem Cell Res. Ther. 10 (1) (2019) 340.

[11] C. Capelli, E. Gotti, M. Morigi, C. Rota, L. Weng, F. Dazzi, O. Spinelli, G. Cazzaniga, R. Trezzi, A. Gianatti, A. Rambaldi, J. Golay, M. Introna, Minimally manipulated whole human umbilical cord is a rich source of clinical-grade human mesenchymal stromal cells expanded in human platelet lysate, Cytotherapy 13 (7) (2011) 786–801.

[12] L. Zhao, M.D. Weir, H.H. Xu, An injectable calcium phosphate-alginate hydrogel-umbilical cord mesenchymal stem cell paste for bone tissue engineering, Biomaterials 31 (25) (2010) 6502–6510.

[13] H.J. Jin, Y.K. Bae, M. Kim, S.J. Kwon, H.B. Jeon, S.J. Choi, S.W. Kim, Y.S. Yang, W. Oh, J.W. Chang, Comparative analysis of human mesenchymal stem cells from bone marrow, adipose tissue, and umbilical cord blood as sources of cell therapy, Int. J. Mol. Sci. 14 (9) (2013) 17986–18001.

[14] S. Kern, H. Eichler, J. Stoeve, H. Klüter, K. Bieback, Comparative analysis of mesenchymal stem cells from bone marrow, umbilical cord blood, or adipose tissue, Stem Cell. 24 (5) (2006) 1294–1301.

[15] R. El Omar, J. Beroud, J.F. Stoltz, P. Menu, E. Velot, V. Decot, Umbilical cord mesenchymal stem cells: the new gold standard for mesenchymal stem cell-based therapies? Tissue Eng. B Rev. 20 (5) (2014) 523–544.

[16] D.C. Ding, Y.H. Chang, W.C. Shyu, S.Z. Lin, Human umbilical cord mesenchymal stem cells: a new era for stem cell therapy, Cell Transplant. 24 (3) (2015) 339–347.

[17] G. Wang, J. Yuan, X. Cai, Z. Xu, J. Wang, D.K.W. Ocansey, Y. Yan, H. Qian, X. Zhang, W. Xu, F. Mao, HucMSC-exosomes carrying miR-326 inhibit neddylation to relieve inflammatory bowel disease in mice, Clin. Transl. Med. 10 (2) (2020) e113.

[18] Y. Sun, H. Shi, S. Yin, C. Ji, X. Zhang, B. Zhang, P. Wu, Y. Shi, F. Mao, Y. Yan, W. Xu, H. Qian, Human mesenchymal stem cell derived exosomes alleviate type 2 diabetes mellitus by reversing peripheral insulin resistance and relieving β-cell destruction, ACS Nano 12 (8) (2018) 7613–7628.

[19] J. Bartolucci, F.J. Verdugo, P.L. González, R.E. Larrea, E. Abarzua, C. Goset, P. Rojo, I. Palma, R. Lamich, P.A. Pedreros, G. Valdivia, V.M. Lopez, C. Nazzal, F. Alcayaga-Miranda, J. Cuenca, M.J. Brobeck, A.N. Patel, F.E. Figueroa, M. Khoury, Safety and efficacy of the intravenous infusion of umbilical cord mesenchymal stem cells in patients with heart failure: a phase 1/2 randomized controlled trial (RIMECARD trial [randomized clinical trial of intravenous infusion umbilical cord mesenchymal stem cells on cardiopathy]), Circ. Res. 121 (10) (2017) 1192–1204.

[20] X. Li, L. Liu, J. Yang, Y. Yu, J. Chai, L. Wang, L. Ma, H. Yin, Exosome derived from human umbilical cord mesenchymal stem cell mediates MiR-181c attenuating burn-induced excessive inflammation, EBioMedicine 8 (2016) 72–82.

[21] S.C. Tao, S.C. Guo, C.Q. Zhang, Modularized extracellular vesicles: the dawn of prospective personalized and precision medicine, Adv. Sci. 5 (2) (2018), 1700449.

[22] Z. Pan, W. Sun, Y. Chen, H. Tang, W. Lin, J. Chen, C. Chen, Extracellular vesicles in tissue engineering: biology and engineered strategy, Adv Healthc Mater (2022), e2201384.

[23] O.P.B. Wiklander, M.Á. Brennan, J. Lötvall, X.O. Breakefield, S. El Andaloussi, Advances in therapeutic applications of extracellular vesicles, Sci. Transl. Med. 11 (492) (2019) eaav8521.

[24] S. Kamerkar, V.S. LeBleu, H. Sugimoto, S. Yang, C.F. Ruivo, S.A. Melo, J.J. Lee, R. Kalluri, Exosomes facilitate therapeutic targeting of oncogenic KRAS in pancreatic cancer, Nature 546 (7659) (2017) 498–503.

[25] Q. Wang, J. Yu, T. Kadungure, J. Beyene, H. Zhang, Q. Lu, ARMMs as a versatile platform for intracellular delivery of macromolecules, Nat. Commun. 9 (1) (2018) 960.

[26] X. Xu, Y. Liang, X. Li, K. Ouyang, M. Wang, T. Cao, W. Li, J. Liu, J. Xiong, B. Li, J. Xia, D. Wang, L. Duan, Exosome-mediated delivery of kartogenin for chondrogenesis of synovial fluid-derived mesenchymal stem cells and cartilage regeneration, Biomaterials 269 (2021), 120539.

[27] L. Alvarez-Erviti, Y. Seow, H. Yin, C. Betts, S. Lakhal, M.J. Wood, Delivery of siRNA to the mouse brain by systemic injection of targeted exosomes, Nat. Biotechnol. 29 (4) (2011) 341–345.

[28] F. Awad, E. Assrawi, C. Louvrier, C. Jumeau, S. Georgin-Lavialle, G. Grateau, S. Amselem, I. Giurgea, S.A. Karabina, Inflammasome biology, molecular pathology and therapeutic implications, Pharmacol. Ther. 187 (2018) 133–149.

[29] X. Cai, Z.Y. Zhang, J.T. Yuan, D.K.W. Ocansey, Q. Tu, X. Zhang, H. Qian, W.R. Xu, W. Qiu, F. Mao, hucMSC-derived exosomes attenuate colitis by regulating macrophage pyroptosis via the miR-378a-5p/NLRP3 axis, Stem Cell Res. Ther. 12 (1) (2021) 416.

[30] X. Zhang, Y. Zhang, R. Li, L. Zhu, B. Fu, T. Yan, Salidroside ameliorates Parkinson's disease by inhibiting NLRP3-dependent pyroptosis, Aging (Albany NY) 12 (10) (2020) 9405–9426.

[31] S. Toldo, A. Abbate, The NLRP3 inflammasome in acute myocardial infarction, Nat. Rev. Cardiol. 15 (4) (2018) 203–214.

[32] M.S.J. Mangan, E.J. Olhava, W.R. Roush, H.M. Seidel, G.D. Glick, E. Latz, Targeting the NLRP3 inflammasome in inflammatory diseases, Nat. Rev. Drug Discov. 17 (8) (2018) 588–606.

[33] A.R. Johnson, J.J. Milner, L. Makowski, The inflammation highway: metabolism accelerates inflammatory traffic in obesity, Immunol. Rev. 249 (1) (2012) 218–238.

[34] W.T. He, H. Wan, L. Hu, P. Chen, X. Wang, Z. Huang, Z.H. Yang, C.Q. Zhong, J. Han, Gasdermin D is an executor of pyroptosis and required for interleukin-1β secretion, Cell Res. 25 (12) (2015) 1285–1298.

[35] I.S. Afonina, Z. Zhong, M. Karin, R. Beyaert, Limiting inflammation-the negative regulation of NF-κB and the NLRP3 inflammasome, Nat. Immunol. 18 (8) (2017) 861–869.

[36] M.J. McAllister, M. Chemaly, A.J. Eakin, D.S. Gibson, V.E. McGilligan, NLRP3 as a potentially novel biomarker for the management of osteoarthritis, Osteoarthritis Cartilage 26 (5) (2018) 612–619.

[37] Z. He, P. Nie, J. Lu, Y. Ling, J. Guo, B. Zhang, J. Hu, J. Liao, J. Gu, B. Dai, Z. Feng, Less mechanical loading attenuates osteoarthritis by reducing cartilage degeneration, subchondral bone remodelling, secondary inflammation, and activation of NLRP3 inflammasome, Bone Joint Res 9 (10) (2020) 731–741.

[38] A.E. Denoble, K.M. Huffman, T.V. Stabler, S.J. Kelly, M.S. Hershfield, G. E. McDaniel, R.E. Coleman, V.B. Kraus, Uric acid is a danger signal of increasing risk for osteoarthritis through inflammasome activation, Proc. Natl. Acad. Sci. U. S. A. 108 (5) (2011) 2088–2093.

[39] Z. Chen, H. Zhong, J. Wei, S. Lin, Z. Zong, F. Gong, X. Huang, J. Sun, P. Li, H. Lin, B. Wei, J. Chu, Inhibition of Nrf2/HO-1 signaling leads to increased activation of the NLRP3 inflammasome in osteoarthritis, Arthritis Res. Ther. 21 (1) (2019) 300.

[40] T. Liu, Q. Zhang, J. Zhang, C. Li, Y.-R. Miao, Q. Lei, Q. Li, A.-Y. Guo, EVmiRNA: a database of miRNA profiling in extracellular vesicles, Nucleic Acids Res. 47 (D1) (2019) D89–D93.

[41] H. Chen, Z. Qin, J. Zhao, Y. He, E. Ren, Y. Zhu, G. Liu, C. Mao, L. Zheng, Cartilage-targeting and dual MMP-13/pH responsive theranostic nanoprobes for osteoarthritis imaging and precision therapy, Biomaterials 225 (2019), 119520.

[42] S. Xue, X. Zhou, W. Sang, C. Wang, H. Lu, Y. Xu, Y. Zhong, L. Zhu, C. He, J. Ma, Cartilage-targeting peptide-modified dual-drug delivery nanoplatform with NIR laser response for osteoarthritis therapy, Bioact. Mater. 6 (8) (2021) 2372–2389.

[43] D.A. Rothenfluh, H. Bermudez, C.P. O'Neil, J.A. Hubbell, Biofunctional polymer nanoparticles for intra-articular targeting and retention in cartilage, Nat. Mater. 7 (3) (2008) 248–254.

[44] R. Largo, M.A. Alvarez-Soria, I. Díez-Ortego, E. Calvo, O. Sánchez-Pernaute, J. Egido, G. Herrero-Beaumont, Glucosamine inhibits IL-1beta-induced NFkappaB activation in human osteoarthritic chondrocytes, Osteoarthritis Cartilage 11 (4) (2003) 290–298.

[45] S.H. Chang, D. Mori, H. Kobayashi, Y. Mori, H. Nakamoto, K. Okada, Y. Taniguchi, S. Sugita, F. Yano, U.I. Chung, J.R. Kim-Kaneyama, M. Yanagita, A. Economides, E. Canalis, D. Chen, S. Tanaka, T. Saito, Excessive mechanical loading promotes osteoarthritis through the gremlin-1-NF-κB pathway, Nat. Commun. 10 (1) (2019) 1442.

[46] T. Li, S. Chubinskaya, A. Esposito, X. Jin, L. Tagliafierro, R. Loeser, A. A. Hakimiyan, L. Longobardi, H. Ozkan, A. Spagnoli, TGF-β type 2 receptor-mediated modulation of the IL-36 family can be therapeutically targeted in osteoarthritis, Sci. Transl. Med. 11 (491) (2019).

[47] T. Matsushita, H. Sasaki, K. Takayama, K. Ishida, T. Matsumoto, S. Kubo, T. Matsuzaki, K. Nishida, M. Kurosaka, R. Kuroda, The overexpression of SIRT1 inhibited osteoarthritic gene expression changes induced by interleukin-1β in human chondrocytes, J. Orthop. Res. 31 (4) (2013) 531–537.

[48] K. Li, Y. Zhang, Y. Zhang, W. Jiang, J. Shen, S. Xu, D. Cai, J. Shen, B. Huang, M. Li, Q. Song, Y. Jiang, A. Liu, X. Bai, Tyrosine kinase Fyn promotes osteoarthritis by activating the β-catenin pathway, Ann. Rheum. Dis. 77 (6) (2018) 935–943.

[49] J.E. Huh, B.K. Seo, Y.H. Baek, S. Lee, J.D. Lee, D.Y. Choi, D.S. Park, Standardized butanol fraction of WIN-34B suppresses cartilage destruction via inhibited production of matrix metalloproteinase and inflammatory mediator in osteoarthritis human cartilage explants culture and chondrocytes, BMC Compl. Alternative Med. 12 (2012) 256.

[50] S.S. Glasson, R. Askew, B. Sheppard, B. Carito, T. Blanchet, H.L. Ma, C.R. Flannery, D. Peluso, K. Kanki, Z. Yang, M.K. Majumdar, E.A. Morris, Deletion of active ADAMTS5 prevents cartilage degradation in a murine model of osteoarthritis, Nature 434 (7033) (2005) 644–648.

[51] L. Zhang, J. Qiu, J. Shi, S. Liu, H. Zou, MicroRNA-140-5p represses chondrocyte pyroptosis and relieves cartilage injury in osteoarthritis by inhibiting cathepsin B/Nod-like receptor protein 3, Bioengineered 12 (2) (2021) 9949–9964.

[52] V.A.K. Rathinam, F.K. Chan, Inflammasome, inflammation, and tissue homeostasis, Trends Mol. Med. 24 (3) (2018) 304–318.

[53] H.C. Dong, P.N. Li, C.J. Chen, X. Xu, H. Zhang, G. Liu, L.J. Zheng, P. Li, Sinomenine attenuates cartilage degeneration by regulating miR-223-3p/NLRP3 inflammasome signaling, Inflammation 42 (4) (2019) 1265–1275.

[54] L. Pan, B. Yan, J. Zhang, P. Zhao, Y. Jing, J. Yu, J. Hui, Q. Lu, Mesenchymal stem cells-derived extracellular vesicles-shuttled microRNA-223-3p suppress lipopolysaccharide-induced cardiac inflammation, pyroptosis, and dysfunction, Int. Immunopharm. 110 (2022), 108910.

[55] T. Paixao, M.D. DiFranco, R. Ljuhar, D. Ljuhar, C. Goetz, Z. Bertalan, H.P. Dimai, S. Nehrer, A novel quantitative metric for joint space width: data from the Osteoarthritis Initiative (OAI), Osteoarthritis Cartilage 28 (8) (2020) 1055–1061.

[56] S.A. Lee, B.R. Park, S.M. Moon, J.H. Hong, D.K. Kim, C.S. Kim, Chondroprotective effect of cynaroside in IL-1β-induced primary rat chondrocytes and organ explants via NF-κB and MAPK signaling inhibition, Oxid. Med. Cell. Longev. 2020 (2020), 9358080.

[57] A. Purushothaman, Exosomes from cell culture-conditioned medium: isolation by ultracentrifugation and characterization, Methods Mol. Biol. 1952 (2019) 233–244.

[58] P. Chen, C. Xia, S. Mei, J. Wang, Z. Shan, X. Lin, S. Fan, Intra-articular delivery of sinomenium encapsulated by chitosan microspheres and photo-crosslinked GelMA hydrogel ameliorates osteoarthritis by effectively regulating autophagy, Biomaterials 81 (2016) 1–13.

[59] K.P. Pritzker, S. Gay, S.A. Jimenez, K. Ostergaard, J.P. Pelletier, P.A. Revell, D. Salter, W.B. van den Berg, Osteoarthritis cartilage histopathology: grading and staging, Osteoarthritis Cartilage 14 (1) (2006) 13–29.

[60] H.J. Mankin, H. Dorfman, L. Lippiello, A. Zarins, Biochemical and metabolic abnormalities in articular cartilage from osteo-arthritic human hips. II. Correlation of morphology with biochemical and metabolic data, J Bone Joint Surg Am 53 (3) (1971) 523–537.